A Robust Reference Optical Spectrum Based in-Band OSNR Monitoring Method Suitable for Flexible Optical Networks
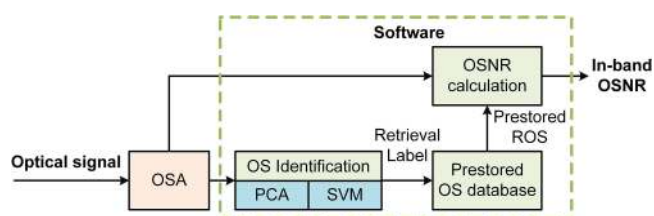
Yibo Zhong
Sheng Cui
Hongwei Lu
Changjian Ke
Haoyu Wang
Peishan Jiang
Deming Liu

The setup of the OSNR monitoring system based on OS identification technique.

A Robust Reference Optical Spectrum Based in-Band OSNR Monitoring Method Suitable for Flexible Optical Networks

Yibo Zhong [ORCID]**,**[1,2] **Sheng Cui** [ORCID]**,**[1,2] **Hongwei Lu,**[1,2] **Changjian Ke,**[1,2] **Haoyu Wang,**[1,2] **Peishan Jiang,**[1,2] **and Deming Liu**[1,2]

[1]Wuhan National Laboratory for Optoelectronics and School of Optical and Electronic Information, Huazhong University of Science & Technology, Wuhan 430074, China
[2]National Engineering Laboratory for Next Generation Internet Access System, Huazhong University of Science & Technology, Wuhan 430074, China

Abstract: The in-band OSNR monitoring methods based on the noise-free reference optical spectrum (ROS) have attracted much attention in the field of optical performance monitoring because they are cost-effective and insensitive to chromatic dispersion and polarization mode dispersion. In this paper, we propose a new ROS based in-band OSNR monitoring method that is robust to the distortions due to non-ideal modulation, the variations of the in-line EDFA gain and the number of filtering elements traversed by the signal. Moreover, this method supports using the standard ROS retrieved by the existing machine-learning technique based optical spectrum identification technique, and thus can remove the need to measure the ROS near the transmitter, which is hard to perform, especially in flexible optical networks. These merits make the method more robust and convenient to use in practice. Extensive numerical simulations are presented to demonstrate the merits of the proposed method with respect to the existing ROS based methods.

Index Terms: Optical signal to noise ratio (OSNR), optical performance monitoring (OPM), optical spectrum (OS), cascaded filtering effect (CFE).

1. Introduction

Optical performance monitoring (OPM) is an enabling technique for robust and intelligent optical networks [1]. Among the list of OPM parameters, optical signal to noise ratio (OSNR) is the most important one because bit error rate (BER) is mainly determined by OSNR when the other transmission distortions, such as chromatic dispersion (CD) and polarization mode dispersion (PMD), are compensated in the digital coherent optical receivers [2]. The traditional OSNR monitoring method using optical spectrum analyzers (OSA) is based on linear interpolation of the noise level from the spectral gaps between signals [3]. But for ultra-dense wavelength division multiplexing (UDWDM) or superchannel transmission systems the spectral gap is very narrow, making the spectral gap blurred or even invisible in common diffraction-grating based OSAs due to the limited resolution (about 0.02 nm) [4]. Furthermore, due to the cascaded filtering effect (CFE) caused by the optical filtering elements contained in the optical nodes, such as optical add-drop multiplexers (OADM)

or wavelength selective switches (WSS), the ASE noise at the spectral gap may be significantly suppressed [5], making the interpolation based method ineffective.

To solve this problem, many in-band OSNR monitoring methods have been proposed [6]–[10]. These methods can be mainly classified into two categories. The first type utilizes linear or nonlinear optical schemes, such as the polarization-nulling technique [6], an optical delay interferometer (ODI) [7], a non-linear loop mirror [8], a fiber parametric device [9], [10] or an optical detector designed for two-photon absorption [11]. The second type of methods relies on digital coherent optical receivers [12]–[14]. Each of these methods has some pros and cons. For the first type of methods, they are cost-effective for network-wide deployment because they are relatively simple in hardware implementations. But some of them are not effective to dual-polarization signals and the others have a relatively small tolerance to the transmission distortions, such as CD and PMD [6]–[10]. For the second type of methods, they have large tolerance to CD and PMD because advanced DSP algorithms can be applied to mitigate the impact of these distortions in advance [12]–[14]. However, with these methods OSNR can only be monitored within the full-fledged digital coherent optical receivers, which are not cost-effective for the network-wide deployment.

Recently reference optical spectrum (ROS) based in-band OSNR monitoring methods have attracted much attention as they are more cost-effective and robust [15]–[20]. These methods rely on the widely deployed OSA [15] or just a simple tunable optical band-pass filter (OBPF) in combination with an optical power meter [18]. They are inherently suitable for dual-polarization signals and insensitive to CD, PMD and fiber nonlinear effect (NLE) [18]. They are also robust to CFE after taking the spectral transmission coefficients of the filtering elements into consideration [19]–[21]. However, the existing ROS based methods are based on three implicit assumptions. The first is that the noise-free ROS keeps invariant after being measured [19], [21]. The second is that the in-line EDFA gain is fixed and equal to the span loss exactly. The third is that the filtering element is present in every span [21]. However, in practice, the unwanted non-ideal modulation (NIM) distortions caused by optical modulator bias voltage drift (BVD), extinction ratio degeneration (ERD) and drive voltage swing variation (DVSV) occur frequently and may change over time due to component defects, environment changes and component aging [22], [23]. Thus, the noise-free ROS launched by the transmitter is not invariant, and may vary with time. With regard to the second assumption, the gain of the in-line EDFA may drift from the nominal value because of manufacture tolerance, working condition and environment changes [24]. With regard to the third assumption, the filtering element may be not present in some spans as OADM or WSS are not always required in every span. Furthermore, the number of the filtering elements traversed by the optical signal may change due to optical path reconfiguration in the flexible networks. Thus, we need to investigate the performance of the existing methods when these assumptions are not valid. Moreover, an obvious shortcoming of the existing ROS based methods is that they need to measure the noise-free ROS near the transmitter. This is inconvenient and hard to perform, especially in the flexible heterogeneous networks where the optical signal propagation path and the type of the received signal optical spectrum (OS) may change frequently over time.

In this paper, we propose a new ROS based in-band OSNR monitoring method that is more robust to the NIM distortions, the variations of the in-line EDFA gain and the number of filtering elements traversed by the signal. Moreover, this method can remove the need to measure the noise-free ROS near the transmitter and support using the standard ROS retrieved by the exiting machine-learning technique based optical spectrum identification technique [25]. Extensive numerical simulations are presented to illustrate the merits of the proposed method with respect to the existing ones when NIM are present and when the in-line EDFA gain and the number of filtering elements are changed.

2. Principle of Operation

The working principle of the ROS based OSNR monitoring method is schematically shown in Fig. 1. Fig. 1(a) depicts the noise-free ROS. In theory, it is only determined by the type of optical signal including its modulation format, baud rate B and pulse shape [25]. As shown in Fig. 1(a), f_{CF} and
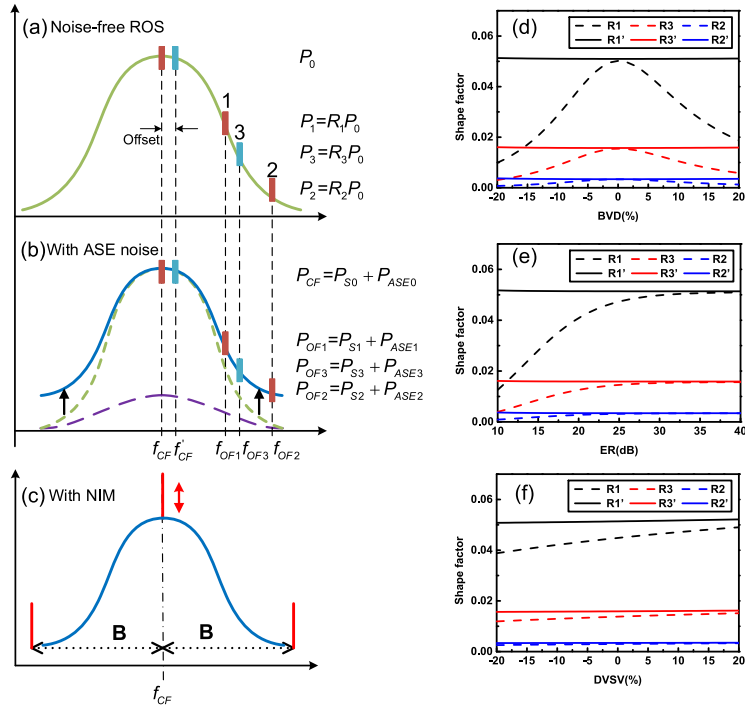
Fig. 1. The working principles of the proposed ROS based OSNR monitoring method (a-c) and the variations of the shape factors as the function of BVD, DVSV and ER (d-f).

$f_{OF1,2,3}$ stand for the optical signal center frequency and three offset frequencies from f_{CF}, while $P_{0,1,2,3}$ stand for the spectral powers measured within a bandwidth of B_w at the frequencies of f_{CF} and $f_{OF1,2,3}$. Thus, under ideal conditions, the ROS shaping factors $R_1 = P_1/P_0$, $R_2 = P_2/P_0$ and $R_3 = P_3/P_0$ are invariant for a given signal type. Fig. 1(b) depicts the signal OS (blue solid line) when ASE noise is present. The spectra of the noise-free ROS (green dashed line) and amplified spontaneous emission (ASE) noise (purple dashed line) are plotted separately for reference. We stress that the ASE spectrum is not flat even inside the signal bandwidth because CFE shapes the signal OS as well as the in-band ASE noise OS [21]. As we can see from Fig. 1(b), OSNR degradation due to ASE noise makes the lower part of the signal OS submerge below the noise pedestal, and meanwhile reduces the slope of the OS edge.

Taking advantage of the spectral shape variation due to ASE noise, the in-band OSNR can be estimated by measuring the spectral power P_{CF} and $P_{OF1,2,3}$ at f_{CF} and $f_{OF1,2,3}$ and solving the equations as follows

$$P_{CF} = P_{S0} + P_{ASE0}, \tag{1}$$

$$P_{OF1} = P_{S1} + P_{ASE1} = R_1 \cdot \alpha^N \cdot P_{S0} + P_{ASE1}, \tag{2}$$

$$P_{OF2} = P_{S2} + P_{ASE2} = R_2 \cdot \beta^N \cdot P_{S0} + P_{ASE2}, \tag{3}$$

$$P_{OF3} = P_{S3} + P_{ASE3} = R_3 \cdot \gamma^N \cdot P_{S0} + P_{ASE3}. \tag{4}$$

Here α, β and γ are used to characterize CFE on the signal spectral shape and stand for the transmission coefficients of the filtering elements at $f_{OF1,2,3}$ respectively. N stands for the number of the filtering elements traversed by the optical signal. Considering that ASE OS is not flat inside the signal bandwidth, $P_{ASE0,1,2,3}$ are not equal and have to be considered as four different variables.

To solve the six unknown variables P_{S0}, $P_{ASE0,1,2,3}$ and N from Eqs. (1)–(4), we assume that there is a linear interpolation relationship between $P_{ASE0,1,2,3}$ as follows

$$\frac{P_{ASE0} - P_{ASE2}}{f_{CF} - f_{OF_2}} = \frac{P_{ASE0} - P_{ASE1}}{f_{CF} - f_{OF_1}}, \tag{5}$$

$$\frac{P_{ASE0} - P_{ASE2}}{f_{CF} - f_{OF_2}} = \frac{P_{ASE0} - P_{ASE3}}{f_{CF} - f_{OF_3}}. \tag{6}$$

With Eqs. (1)–(4), (5) and (6), the six unknown variables P_{S0}, $P_{ASE0,1,2,3}$ and N can be solved. Finally, the in-band OSNR can be calculated using the following equation

$$OSNR = 10 \log_{10} \left(\kappa \frac{P_{S0}}{P_{ASE0}} \right). \tag{7}$$

where the calibration parameter κ is determined by B_w and signal bandwidth.

For comparison, the existing ROS based methods only utilize Eqs. (1)–(3) to estimate the in-band OSNR as they have some loose assumptions such as the ASE noise OS is flat ($P_{ASE0,1,2,3}$ are equal) [19], or the received ASE noise spectral powers can be modeled with a geometric sequence with common ratios of α and β based on the second and third assumptions aforementioned [21]. Furthermore, all existing ROS based methods assume that the noise-free ROS and thus the shape factors $R_{1,2,3}$ are invariant after the ROS is measured near the transmitter. However, in practice the height of the spectral line (the impulse) at f_{CF} corresponding to the optical carrier component may vary over time due to NIM effect including BVD, ERD and DVSV, as shown in Fig. 1(c) [24], [25]. In theory, the spectral line only exists in the amplitude shift keying (ASK) signal OS and does not occur in the mPSK and mQAM signal OS. This is because the commonly used mPSK and mQAM constellations are symmetric relative to the origin of the complex plane and thus the optical carrier component is completely suppressed as the alphabet consists of counter-phase symbols [26]. However, NIM will distort the constellation symmetry to some extent, and thus the optical carrier component at f_{CF} will appear and vary randomly. In other words, P_0 is affected by the NIM distortions and will change over time for the same reason. This issue makes the shaping factors $R_{1,2,3}$ also dependent on the NIM and related to a specific transmitter with its own NIM patterns (combinations of BVD, ERD and DVSV). So ROS must be measured near the corresponding transmitter. Furthermore, $R_{1,2,3}$ will change over time. Thus, the solutions of the equations may be incorrect or even do not exist in some cases. To mitigate the impact of the NIM effect, we measure P_0 and P_{CF} at f'_{CF} which has a small offset Δf from f_{CF} as shown in Fig. 1(a) and (b). When $\Delta f > B_w$ the effect of the central spectral line and thus NIM will be mitigated. We denoted the new shape factors obtained with this method as $R'_{1,2,3}$.

Fig. 1(d-f) show the variations of $R_{1,2,3}$ and $R'_{1,2,3}$ as the function of BVD, ERD and DVSV for the 25GBaud PM-QPSK signals obtained by numerical simulations. Here BVD and DVSV are defined as the ratios of the deviations to the nominal values [25]. B_w and the offset Δf are set to be 500 MHz and 600 MHz, respectively. As we can see from Fig. 1(d) and (e), when BVD deviates from the ideal value or when ER becomes smaller, $R_{1,2,3}$ decreases because the intensity of the optical carrier component (the central spectral line height) grows with the NIM effect, and thus P_0 becomes larger. But $R'_{1,2,3}$ can maintain nearly the same value. Fig. 1(f) shows that $R_{1,2,3}$ also changes with DVSV, while $R'_{1,2,3}$ is insensitive to the variations of DVSV.

After the above improvement, the shape factors $R'_{1,2,3}$ are not related to a specific transmitter any more. Under this condition, the new method can adopt the standard ROS retrieved from the OS database utilizing the machine-learning based OS identification technique [25]. By this way, we can remove the need to measure the ROS near the transmitter which is very hard to perform in practice. The setup of the ROS based OSNR monitoring system utilizing this technique is shown in Fig. 2. The OS of the optical signal tapped from transmission fiber is first measured with an OSA and then input into the OS type identification module which is based on the integration of two machine learning techniques, namely unsupervised principle component analysis (PCA) and supervised multiclass support vector machines (SVMs) for feature extraction and OS classification,
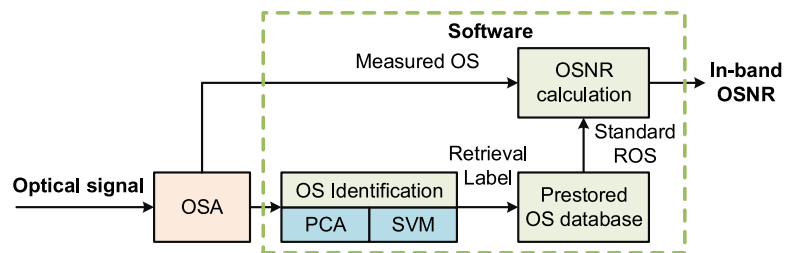
Fig. 2. The setup of the OSNR monitoring system based on OS identification technique.
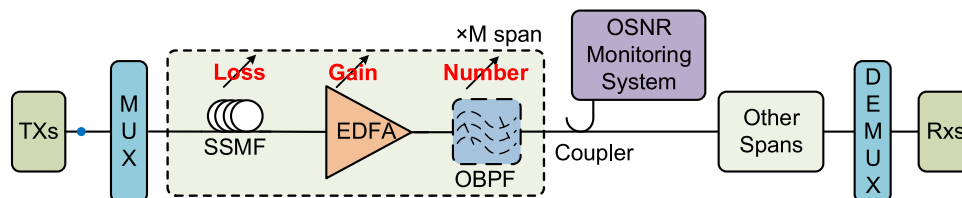

Fig. 3. The setup of the EDFA amplified multi-span 100Gbps dual polarization NRZ-QPSK transmission system.

respectively [25]. The classification label output by the SVM classifier is used to retrieve the standard noise-free ROS from the OS database consisting of ideal distortion-free ROS of the different types of the optical signals appearing in the network [25]. Finally, both of the received OS and retrieved standard ROS are input into the OSNR calculation module to calculate the in-band OSNR. Except the OSA, all of the modules in Fig. 2 can be implemented in software and thus they can be integrated into an OSA without any extra hardware cost.

3. Performance Comparison of Different ROS-Based Methods

The EDFA amplified multi-span 3×100 Gbps dual polarization NRZ-QPSK transmission system shown in Fig. 3 is set up to evaluate the performance of the ROS based methods proposed before and in this paper. The OSNR of the central channel is measured with the methods proposed in [19], [21] and this paper (hereafter referred to as method 1, 2 and 3). The numerical simulations are based on the commercial software VPI TransmissionMaker 9.0. The QPSK signal is generated using the commonly used modulation scheme [27]. OSNR is varied by changing the launched signal power. In every span, a realistic fourth order Gaussian multichannel OBPF model with 50 GHz 3 dB bandwidth has been implemented to apply CFE [5]. It is plotted with dashed lines as they may not exist in every span. Without loss of generality, we assume that the optical signal propagates over 10 spans of 100 km standard single-mode fiber (SSMF) before being tested at the OSNR monitoring point. The attenuation and dispersion coefficients of the SSMF are 0.2 dB/km and 16 ps/nm/km, respectively. In each span, an in-line EDFA is used to compensate the span loss. We note that ASE noise is generated in each of the EDFAs and thus ASE noise, as well as the optical signal, will experience significant CFE before being measured at the monitoring point.

For method 1 and 2, P_{CF,OF_1,OF_2} are measured with $B_w = 500$MHz at f_{CF}, $f_{OF_1} = f_{CF} + 20$ GHz and $f_{OF_2} = f_{CF} + 23.5$ GHz, which are the optimized parameters according to [21]. For method 3, P_{CF} is measured at $f'_{CF} = f_{CF} + 0.6$ GHz and the additional P_{OF_3} is measured at $f_{OF_3} = f_{CF} + 22$ GHz. In this paper we assume that the signal OS is measured with an ultra-high resolution OSA [19], [28]. They can provide a spectral resolution of about 0.1pm (12.5 MHz) [28] and thus can easily satisfy the spectral power measurement requirement with $B_w = 500$ MHz.
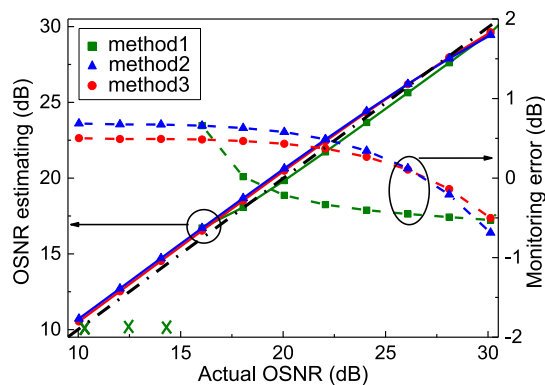
Fig. 4. The variations of the estimated OSNR obtained by the three methods as a function of the real OSNR.

TABLE 1

Different Combinations of NIM Distortions. Here EDFA Gain Variation is not Considered and $N = 10$

	BVD	DVSV	ER(dB)
Case 1	0	0	24
Case 2	8%	0	24
Case 3	16%	0	24
Case 4	0	8%	24
Case 5	0	16%	24
Case 6	8%	8%	20

To demonstrate the different performance of the ROS methods, first, we assume that NIM distortions are not present and the gain of the in-line EDFAs is equal to the span loss exactly and the filtering elements are present in every span ($N = 10$). Fig. 4 shows the variations of the estimated OSNR as a function of the real ones obtained by method 1, 2 and 3. As we can see, under this ideal condition the performance is similar for methods 1, 2 and 3 when OSNR is higher than 15 dB. But method 1 doesn't work (no solutions of Eqs. (1)–(3) exist) when OSNR is below 15 dB because it assumes that $P_{ASE0,1,2}$ are equal [19]. Thus, in the following investigation we only compare methods 2 and 3 that perform well in Fig. 4. It is noteworthy that the calibration parameter κ is set at 1.35 and 1.05 dB for method 2 and 3, respectively, and no recalibration is carried out for both of them in the following test.

To investigate the impact of NIM distortions, the six cases with different combinations of BVD, DVSV and ER listed in Table 1 are considered in the test. Fig. 5 shows the monitoring results obtained by method 2 and 3 when the shape factors measured in case 1 is used to estimate the OSNR for the other cases. Fig. 5(a) shows the variations of the estimated OSNR as a function of the real ones. As we can see, the performance of method 2 is satisfactory in case 2 but degrades significantly in case 3, 4, 5 and 6. Fig. 5(b) shows the variations of the estimation error against the real ones. The maximal error is only 1 dB for case 2 while it reaches 4.5 dB for case 5. The insets in Fig. 5(b) can explain the reason. They are the ROS measured in case 2 and 5 when OSNR = 20 dB. As we can see, the two ROS are obviously different and the latter has a much higher spectral line at the center. Fig. 5(c) shows the variations of the estimated OSNR as a function of the real ones when our method is used. As we can see, the curves obtained under different NIM distortions overlapped with each other very well, proving that our method is insensitive to these NIM distortions. Fig. 5(d) shows the variations of the estimation error against the real ones for our method. The maximal error is only about 1 dB for all of the cases.
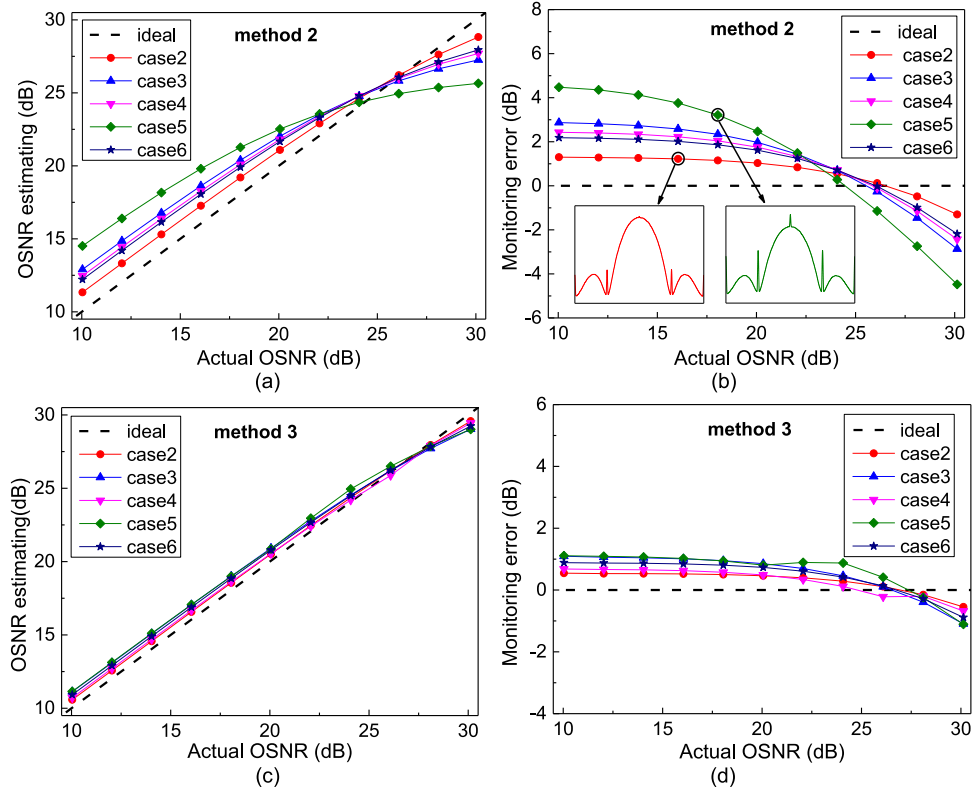
Fig. 5. The variations of the estimated OSNR (a, c) and estimation error (b, d) obtained by method 2 and 3 as a function of the real OSNR. The insets in (b) are two example ROS corresponding to case 2 and case 5, respectively.
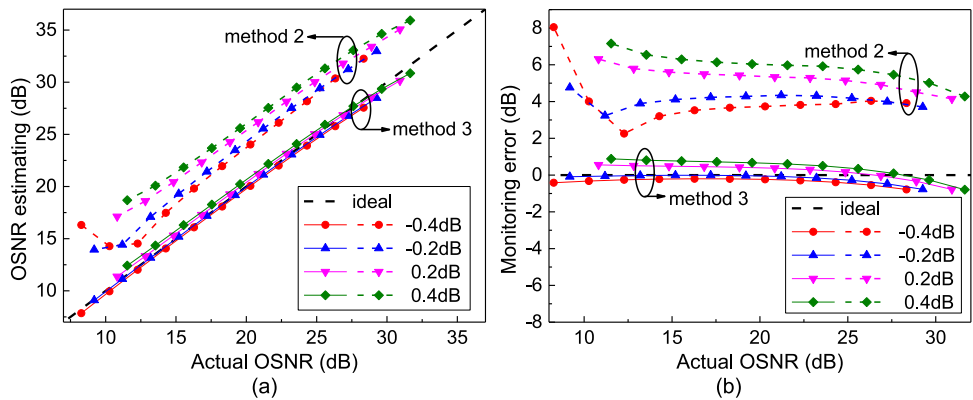

Fig. 6. The monitoring results obtained with method 2 and 3 when the EDFA gain deviates from the nominal value.

The performance of method 2 and 3 is also investigated when the EDFA gain deviates from the nominal value and the filtering elements are not present in some spans. The EDFA gain is changed by ±0.2 and ±0.4 dB from the nominal value according to real fluctuations of the EDFA gain [24]. Fig. 6(a) shows the variations of the estimated OSNR versus the real ones. As we can see, the OSNR estimated with method 2 (dashed lines) deviates from the real value and is not consistent with each other. While with our method the estimated OSNR agrees with the real ones very well in all cases, validating that our method is also insensitive to the EDFA gain variations. Fig. 6(b) shows
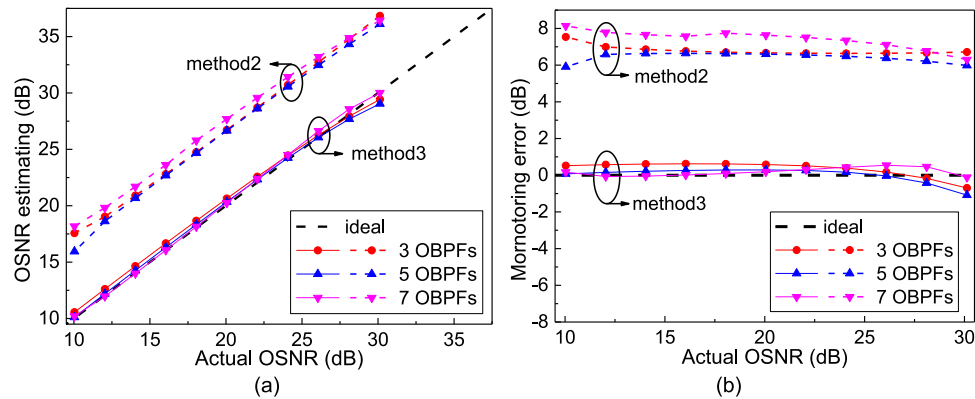
Fig. 7. The monitoring results obtained with methods 2 and 3 when *N* changes.

TABLE 2
Different Combinations of the Three Effects

| | Non-ideal modulation | | | EDFA gain deviation (dB) | N |
	BVD	DVSV	ER(dB)		
Case 7	8%	8%	24	0.2	7
Case 8	8%	0	20	0.2	5
Case 9	16%	8%	20	0.2	7

the variations of the estimation error versus the input signal OSNR. For method 2, the maximal error is about 8 dB. While for our method, the maximal error is still below 1 dB.

Fig. 7(a) shows the variations of the estimated OSNR as a function of the real ones when the number of the filtering elements are 3, 5 and 7, respectively. As we can see, the OSNR estimated with method 2 also deviates from the real ones. While with our method the estimated OSNR still agrees well with the real ones. Fig. 7(b) shows the variations of the estimation error versus the input signal OSNR. For method 2, the maximal error is about 7 dB. While for our method, the maximal error is still about 1 dB. We note that recalibration can't solve the problem for method 2 because the EDFA gain and the number of the filtering elements traversed by the signals may change over time.

In practical applications, the distortions of NIM, the variations of the in-line EDFA gain and the number of filtering elements may coexist. To investigate the overall impact of these effects, three more cases as listed in Table 2 are considered in the test. Compared with Table 1, the variations of the in-line EDFA gain and the number of filtering elements are taken into account. Fig. 8(a) shows the variations of the estimated OSNR obtained with method 2 versus the real OSNR. As we can see, the curves not only become severely bended as in Fig. 5(a), but also move up from the dashed line representing the real OSNR as in Fig. 6(a) and Fig. 7(a). This phenomenon is due to the combining effects of NIM and the variations of the EDFA gain and *N*. Fig. 8(b) shows the estimation error of method 2. The maximal error is about 8 dB. The large error can be avoided using the new method. Fig. 8(a) also shows the estimation results obtained with method 3. As we can see, the estimated OSNR still agrees with the real OSNR very well for all of the three cases. As we can see from Fig. 8(b), the estimation error of the new method only increases to about 2 dB when OSNR reaches 30 dB. The maximal error of the new method is still smaller than 1 dB when OSNR varies from 10 to 26 dB. This region is of greater interest for most practical applications.

We also evaluate the computation complexity of the three methods. Each algorithm runs 100 times on a personal computer for different input OSNRs and combinations of NIM, EDFA gain deviations and *N*. The computer is equipped with an i7-6700HQ CPU and 12 GB memory. All of
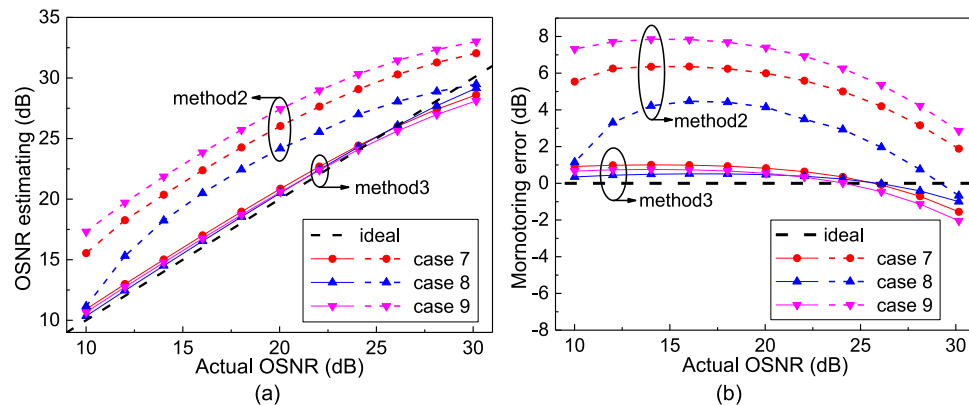
Fig. 8. The monitoring results obtained with methods 2 and 3 when NIM, the variations of the in-line EDFA gain and the number of filtering elements coexist.

the algorithms are implemented in Matlab R2017a using the Matlab function 'fsolve' to solve the equations. For method 1 and 2 they have to solve three equations, while the new method has to solve six equations. The averaged elapsed times for method 1, 2 and 3 are 0.844 s, 0.843 s and 0.846 s, respectively. The time difference is very small, proving that the computation complexities of them are similar.

4. Conclusions

In this paper, we propose a new ROS based OSNR monitoring method that is more robust and convenient to use in practice. We first mitigate the NIM effect on the signal spectral factors by measuring the center spectral power with a small offset from the optical carrier frequency. We then mitigate the effect induced by the variations of the in-line EDFA gain and filtering element number by establishing a new OSNR calculation model without any implicit assumptions about the EDFA gain and filtering element number. Furthermore, the new method makes the spectral factors in the OSNR calculation model not related to a specific transmitter, and thus supports using the pre-stored standard ROS retrieved by the OS identification technique. Thus, it can remove the need to measure the ROS near the transmitter. We also find that the computation complexity of the new method is very close to the exiting methods. These merits make the new method more robust and convenient to use in practice, compared with the existing ones.

References

[1] Z. Dong, F. N. Khan, Q. Sui, K. Zhong, C. Lu, and A. P. T. Lau, "Optical performance monitoring: A review of current and future technologies," *J. Lightw. Technol.*, vol. 34, no. 2, pp. 525–543, Jan. 2016.
[2] S. J. Savory, "Digital coherent optical receivers: Algorithms and subsystems," *IEEE J. Sel. Topics Quantum Electron.*, vol. 16, no. 5, pp. 1164–1179, Sep./Oct. 2010.
[3] Optical Monitoring for Dense Wavelength Division Multiplexing Systems, ITU-T G.697, Nov. 2016. [Online]. Available: https://www.itu.int/rec/T-REC-G.697-201611-I
[4] Yokogawa Test & Measurement Corporation, "AQ6370D telecom optical spectrum analyzer 600-1700 nm," 2019. [Online]. Available: https://tmi.yokogawa.com/solutions/products/optical-measuring-instruments/optical-spectrum-analyzer/aq6370d-optical-spectrum-analyzer/
[5] J. M. Fabrega and M. Svaluto Moreolo, "On the filter narrowing issues in elastic optical networks," *J. Opt. Commun. Netw.*, vol. 8, no. 7, pp. A23–A33, Jul. 2016.
[6] J. H. Lee, D. K. Jung, C. H. Kim, and Y. C. Chung, "OSNR monitoring technique using polarization-nulling method," *IEEE Photon. Technol. Lett.*, vol. 13, no. 1, pp. 88–90, Jan. 2001.
[7] X. Liu, Y. H. Kao, S. Chandrasekhar, I. Kang, S. Cabot, and L. L. Buhl, "OSNR monitoring method for OOK and DPSK based on optical delay interferometer," *IEEE Photon. Technol. Lett.*, vol. 19, no. 15, pp. 1172–1174, Aug. 2007.

[8] R. Adams, M. Rochette, T. T. Ng, and B. J. Eggleton, "All-optical in-band OSNR monitoring at 40 Gb/s using a nonlinear optical loop mirror," *IEEE Photon. Technol. Lett.*, vol. 18, no. 3, pp. 469–471, Feb. 2006.

[9] T. T. Ng, J. L. Blows, M. Rochette, J. A. Bolger, I. Littler, and B. J. Eggleton, "In-band OSNR and chromatic dispersion monitoring using a fibre optical parametric amplifier," *Opt. Express*, vol. 13, no. 14, pp. 5542–5552, Jul. 2005.

[10] S. Cui, S. Sun, L. Li, J. Li, Q. You, and D. Liu, "All-optical in-band optical signal-to-noise monitoring method based on degenerated four-wave mixing," *IET Optoelectronics*, vol. 6, no. 2, pp. 107–109, 2012.

[11] S. Wielandy, M. Fishteyn, B. Zhu, "Optical performance monitoring using nonlinear detection," *J. Lightw. Technol.*, vol. 22, no. 3, pp. 784–793, Mar. 2004.

[12] M. S. Faruk, Y. Mori, and K. Kikuchi, "In-band estimation of optical signal-to-noise ratio from equalized signals in digital coherent receivers," *IEEE Photon. J.*, vol. 4, no. 1, Feb. 2014, Art. no. 7800109.

[13] D. Zhao, L. Xi, X. Tang, W. Zhang, Y. Qiao, and X. Zhang, "Periodic training sequence aided in-band OSNR monitoring in digital coherent receiver," *IEEE Photon. J.*, vol. 6, no. 4, Aug. 2014, Art. no. 7902009.

[14] L. Dou *et al.*, "An accurate nonlinear noise insensitive OSNR monitor," in *Proc. Opt. Fiber Commun. Conf. (Opt. Soc. Amer.)*, Mar. 2016, Paper W3A.5.

[15] D. Gariépy, G. He, and G. W. Schinn, "Non-intrusive measurement of in-band OSNR of high bitrate polarization-multiplexed signals," *Opt. Fiber Technol.*, vol. 17, no. 5, pp. 518–522, Oct. 2011.

[16] D. Gariépy, S. Searcy, G. He, and S. Tibuleac, "Non-intrusive OSNR measurement of polarization-multiplexed signals with spectral shaping and subject to fiber non-linearity with minimum channel spacing of 37.5GHz," *Opt. Express*, vol. 24, no. 18, pp. 20156–20166, Sep. 2016.

[17] D. Gariépy, S. Searcy, G. He, and S. Tibuleac, "Demonstration of non-intrusive in-band OSNR measurement technique for PM-16QAM signals with spectral shaping and subject to fiber nonlinearity," in *Proc. Opt. Fiber Commun. Conf. (Opt. Soc. Amer.)*, Mar. 2016, Paper Tu3G.5.

[18] S. Oda *et al.*, "In-band OSNR monitor using an optical bandpass filter and optical power measurements for superchannel signals," in *Proc. Eur. Conf. Exhib. Opt. Commun.*, Sep. 2013, pp. 1–3.

[19] Z. Dong *et al.*, "Modulation-format-independent OSNR monitoring insensitive to cascaded filtering effects by low-cost coherent receptions and RF power measurements," *Opt. Express*, vol. 23, no. 12, pp. 15971–15982, Jun. 2015.

[20] Z. Huang *et al.*, "A novel in-band OSNR measurement method based on normalized autocorrelation function," *IEEE Photon. J.*, vol. 10, no. 2, Apr. 2018, Art. no. 7903208.

[21] G. Yin, S. Cui, C. Ke, and D. Liu, "Reference optical spectrum based in-band OSNR monitoring method for EDFA amplified multispan optical fiber transmission system with cascaded filtering effect," *IEEE Photon. J.*, vol. 10, no. 3, Jun. 2018, Art. no. 7201910.

[22] X. Zhu, Z. Zheng, C. Zhang, L. Zhu, Z. Tao, and Z. Chen, "Coherent detection-based automatic bias control of Mach–Zehnder modulators for various modulation formats," *J. Lightw. Technol.*, vol. 32, no. 14, pp. 2502–2509, Jul. 2014.

[23] iXBlue Photonics, "Introduction to iXBlue Mach-Zehnder modulators bias controllers," 2019. [Online]. Available: https://photonics.ixblue.com/sites/default/files/2019-01/Introduction%20To%20iXblue%20MBC%202019.pdf

[24] Y. Oikawa, N. Sato, K. Ota, S. Petit, and N. Shiga, "0.2-dB gain excursion AGC-EDFA with a high speed VOA for 100-channel add/drop equivalent operation," in *Proc. Opt. Fiber Commun. Conf. (Opt. Soc. Amer.)*, Mar. 2012, Paper OW4D.3.

[25] H. Lu, S. Cui, C. Ke, and D. Liu, "Automatic reference optical spectrum retrieval method for ultra-high resolution optical spectrum distortion analysis utilizing integrated machine learning techniques," *Opt. Express*, vol. 25, no. 26, pp. 32491–32503, Dec. 2017.

[26] E. Ip and J. M. Kahn, "Power spectra of return-to-zero optical signals," *J. Lightw. Technol.*, vol. 24, no. 3, pp. 1610–1618, Mar. 2006.

[27] P. J. Winzer and R. Essiambre, "Advanced optical modulation formats," in *Optical Fiber Telecommunications V Volume B: Systems and Networks*, I. P. Kaminow, T. Li, and A. E. Willner, Burlington, MA, USA: Elsevier, 2008, ch. 2, pp. 23–93.

[28] C. Xing, C. Ke, K. Zhang, Z. Guo, Y. Zhong, and D. Liu, "Polarization- and wavelength-independent SBS-based filters for high resolution optical spectrum measurement," *Opt. Express*, vol. 25, no. 18, pp. 20969–20982, Sep. 2017.